Science Advances
AAAS

Supplementary Materials for

Semirational bioengineering of AAV vectors with increased potency and specificity for systemic gene therapy of muscle disorders

Jihad El Andari *et al.*

Corresponding author: Dirk Grimm, dirk.grimm@bioquant.uni-heidelberg.de;
Ana Buj-Bello, abujbello@genethon.fr

Sci. Adv. **8**, eabn4704 (2022)
DOI: 10.1126/sciadv.abn4704

This PDF file includes:

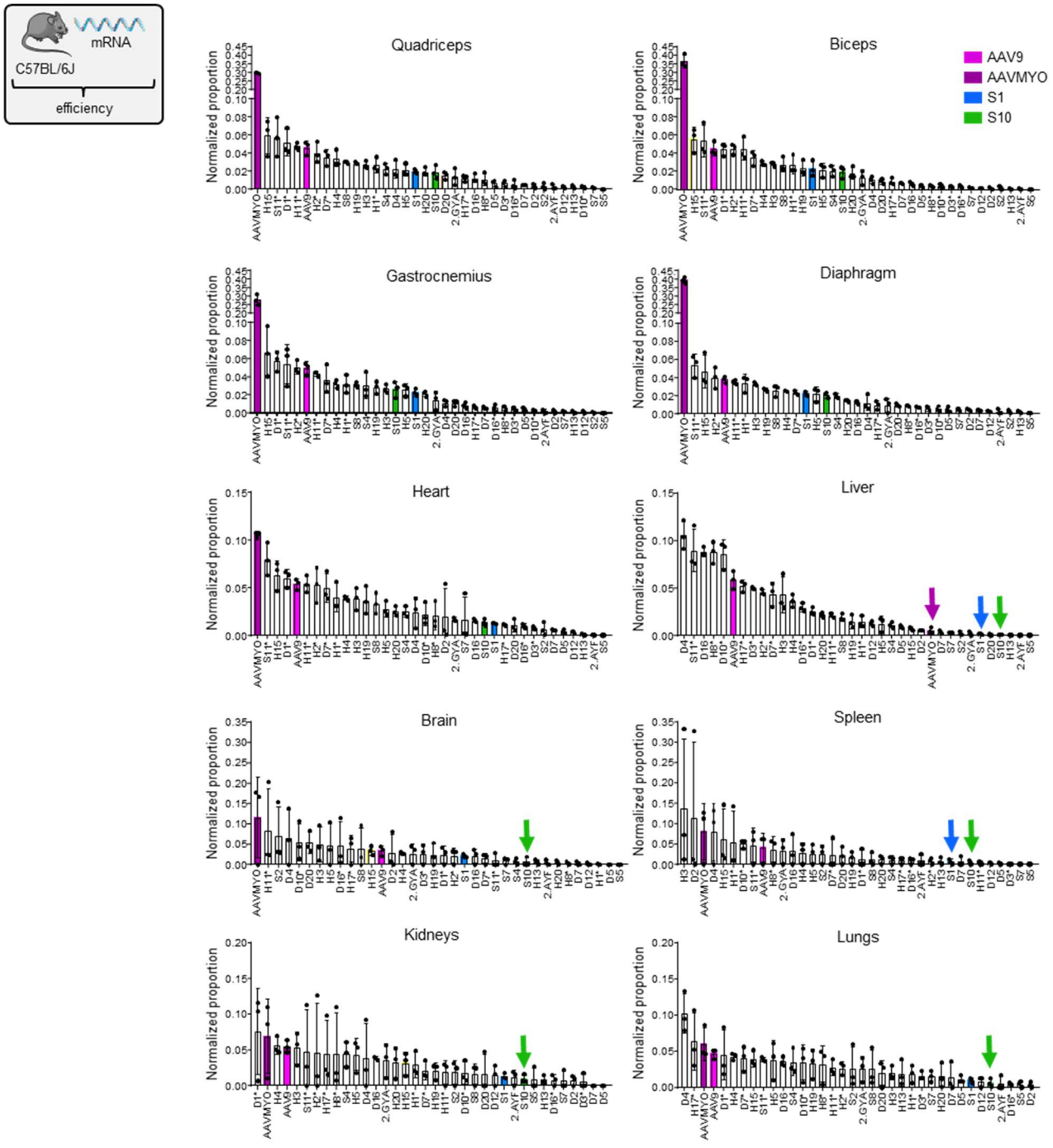

Fig. S1. Transcriptional efficiency of selected AAVs in muscle and other tissues.

All 36 capsids were ranked by normalized transcriptional efficiency ($V_{\alpha\beta}$) in the shown ten tissues. Bars are mean values with SD from three C57BL/6J mice (each mouse is one dot). AAV variants of particular interest in this work are highlighted by colors. 2.AYF, AAV2.ESGHAYF; 2.GYA, AAV2.ESGHGYA. The asterisks indicate AAV variants originating from library B whereas all others are from library A, except for AAV9 and AAVMYO.

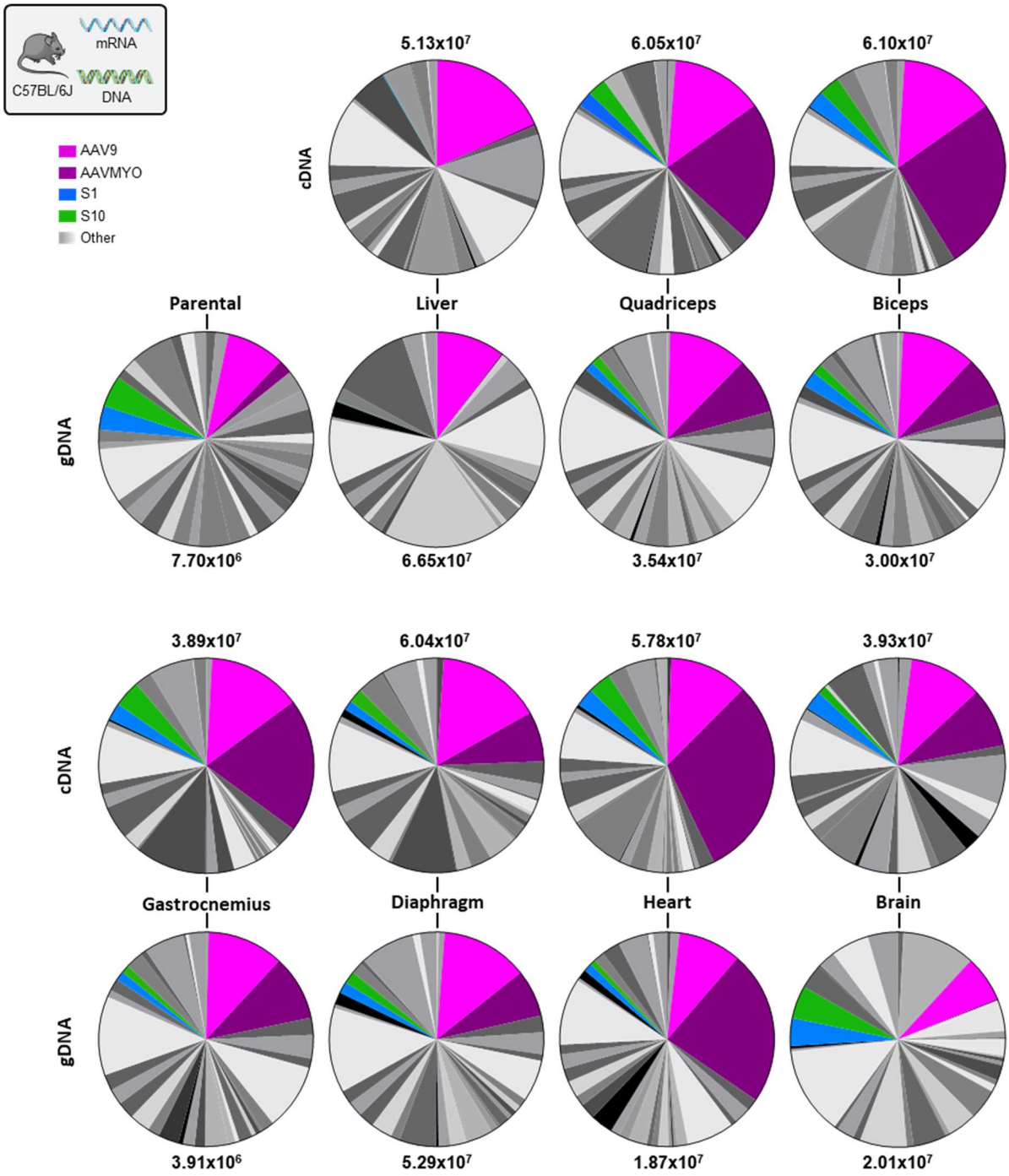

Fig. S2. Proportion of recovered raw reads of a particular barcode in multiple tissues compared to the parental NGS library.

Pie charts depict the percentage of each capsid-specific barcode in a given tissues relative to the sum of all reads in this tissue (numbers above or below the charts, respectively). Total reads per tissue was calculated as the sum of all reads in this tissue in all three C57BL/6J mice. Total reads in the parental library is the sum of all recovered reads of the initial library that was injected into the mice.

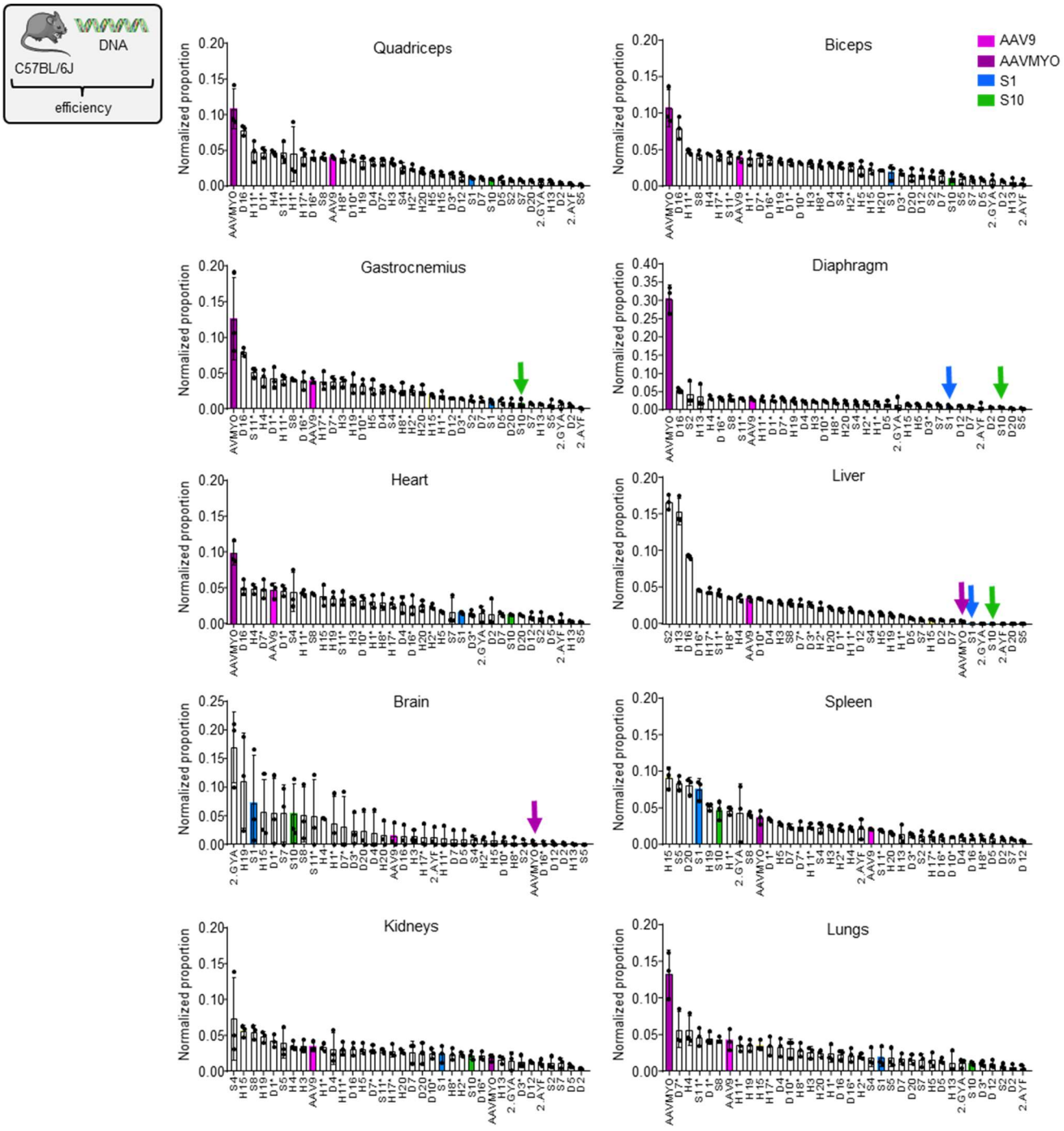

Fig. S3. Transduction efficiency of selected AAVs from evolved shuffled libraries in ten tissues.

All capsids were ranked based on normalized transduction efficiency ($V_{\alpha\beta}$). Depicted are mean DNA values from three C57BL/6J mice with SD. Note that here and in all subsequent figures, "transduction efficiency" is defined as the capability of a given capsid to deliver detectable vector DNA to the target tissue.

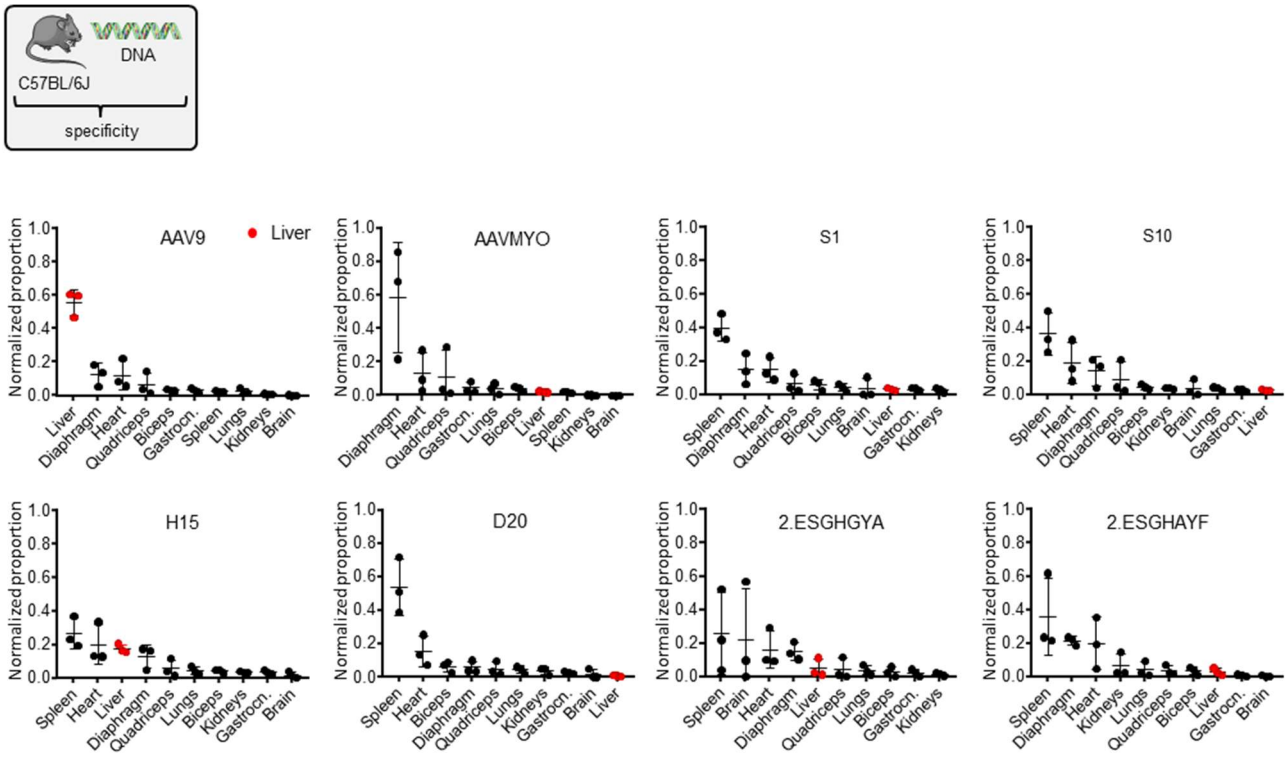

Fig. S4. Transduction specificity of chimeric AAVs and benchmarks.

Depicted are normalized mean DNA values plus SD from three C57BL/6J mice. Liver samples are highlighted in red.

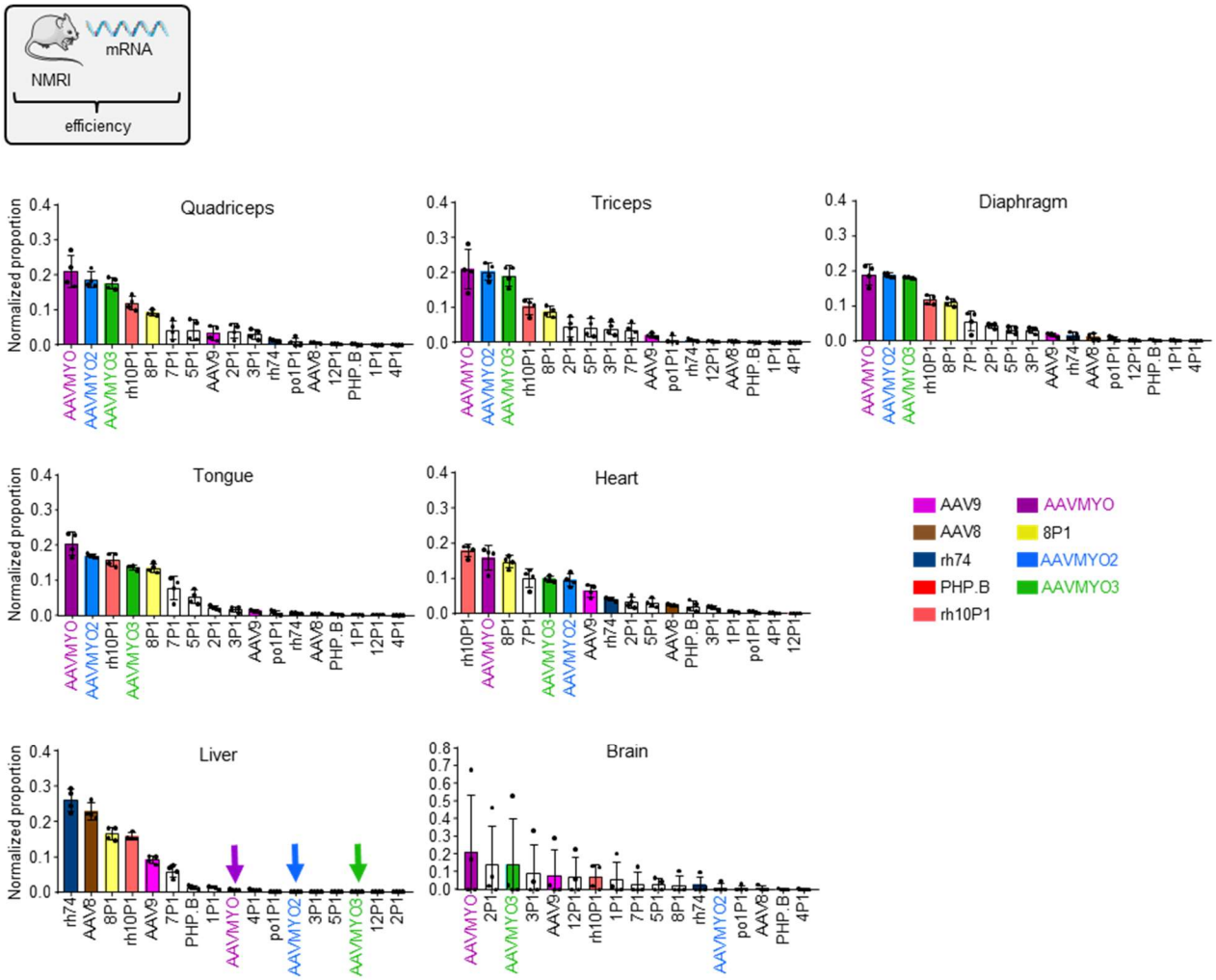

Fig. S5. Transcriptional efficiency of P1-displaying AAVs in multiple tissues in NMRI mice.
Depicted are normalized mean cDNA (mRNA) values plus SD from four NMRI mice. Each dot represents one mouse. AAV variants of particular interest in this work are highlighted by colors.

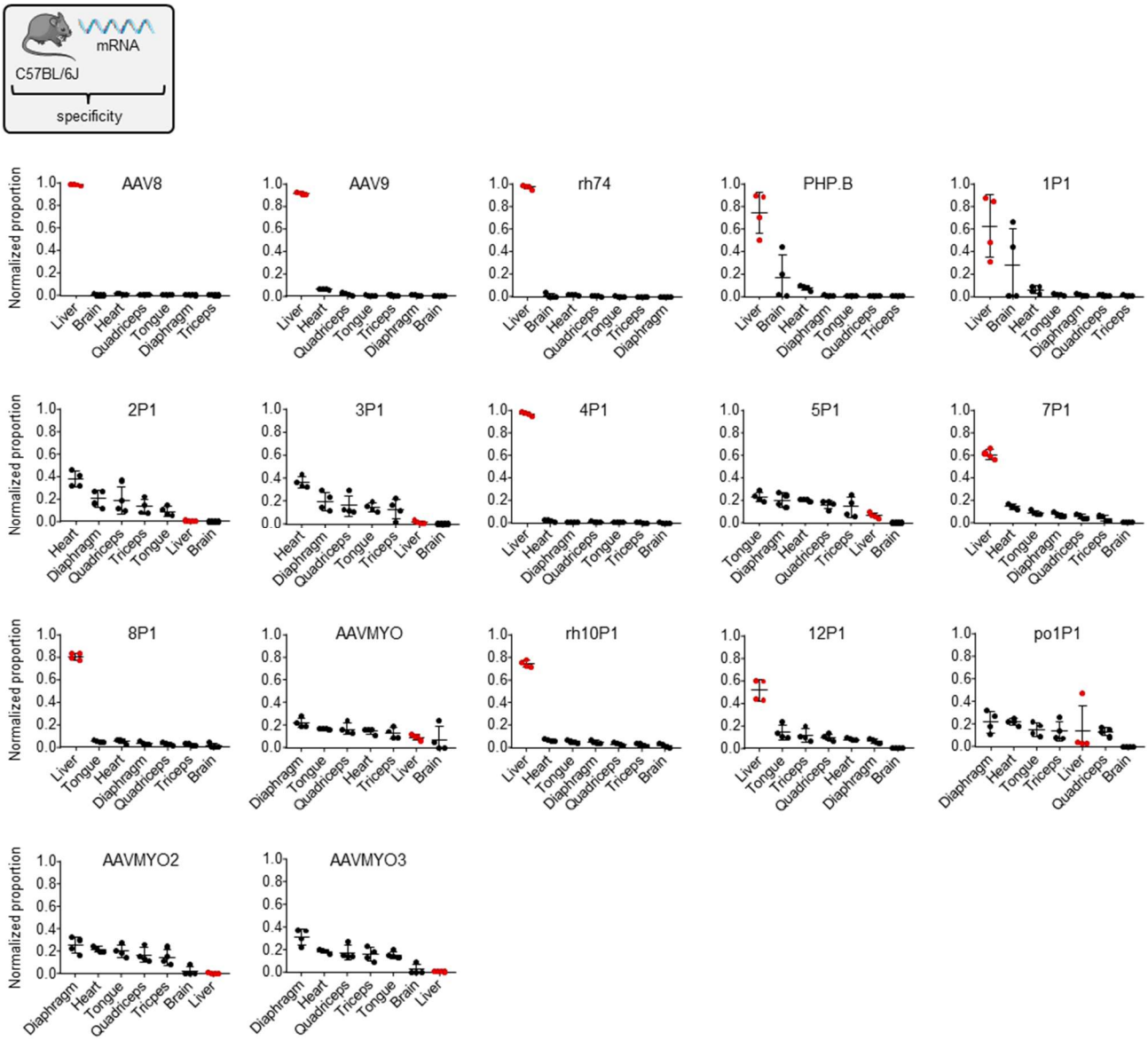

Fig. S6. Transcriptional specificity of P1-displaying AAVs in multiple tissues in C57BL/6J mice.

Shown is the transcriptional specificity ($T_{\alpha\beta}$) of 17 capsids as normalized proportion per cell (diploid genome, dg) in seven tissues. Depicted are mean cDNA (mRNA) values with SD from four C57BL/6J mice. Liver samples are highlighted in red.

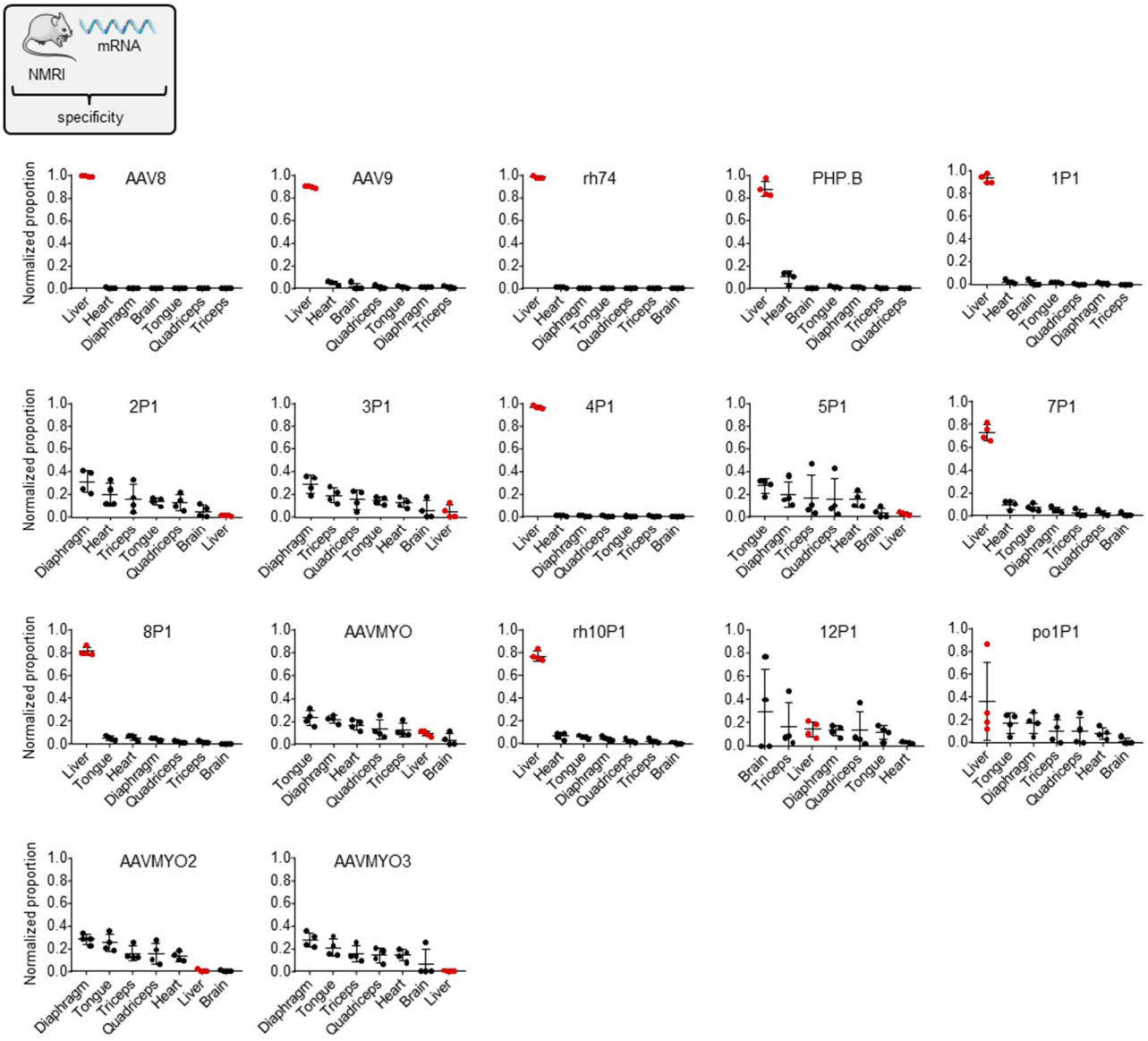

Fig. S7. Transcriptional specificity of P1-displaying AAVs in multiple tissues in NMRI mice.

Shown is the transcriptional specificity ($T_{\alpha\beta}$) of 17 capsids as normalized proportion per cell (diploid genome, dg) in seven tissues. Depicted are mean cDNA values with SD from four NMRI mice. Liver samples are highlighted in red.

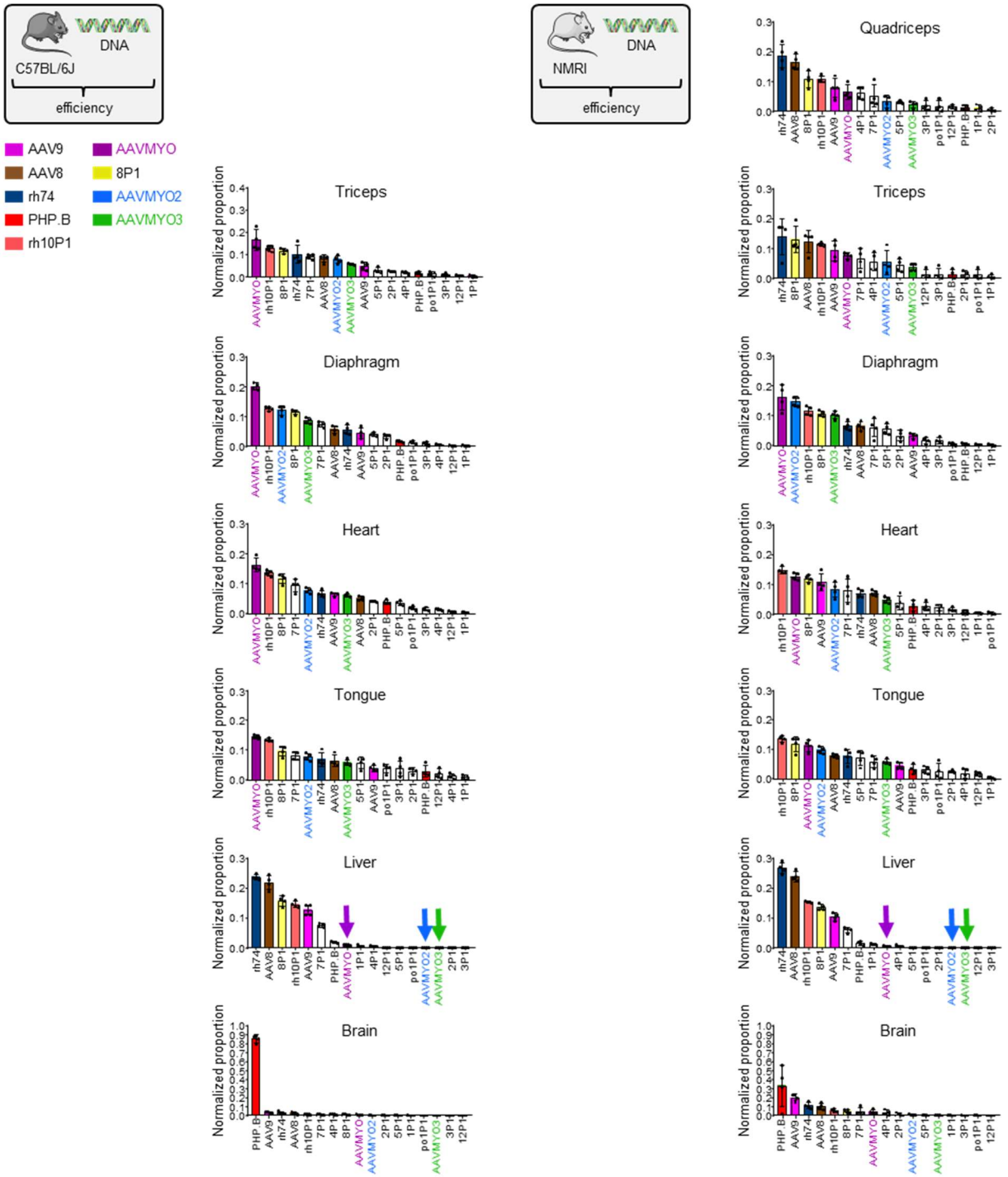

Fig. S8. Transduction efficiency of P1-displaying AAVs in multiple tissues in C57BL/6J or NMRI mice.

Depicted are normalized mean DNA values plus SD from four C57BL/6J or four NMRI mice.

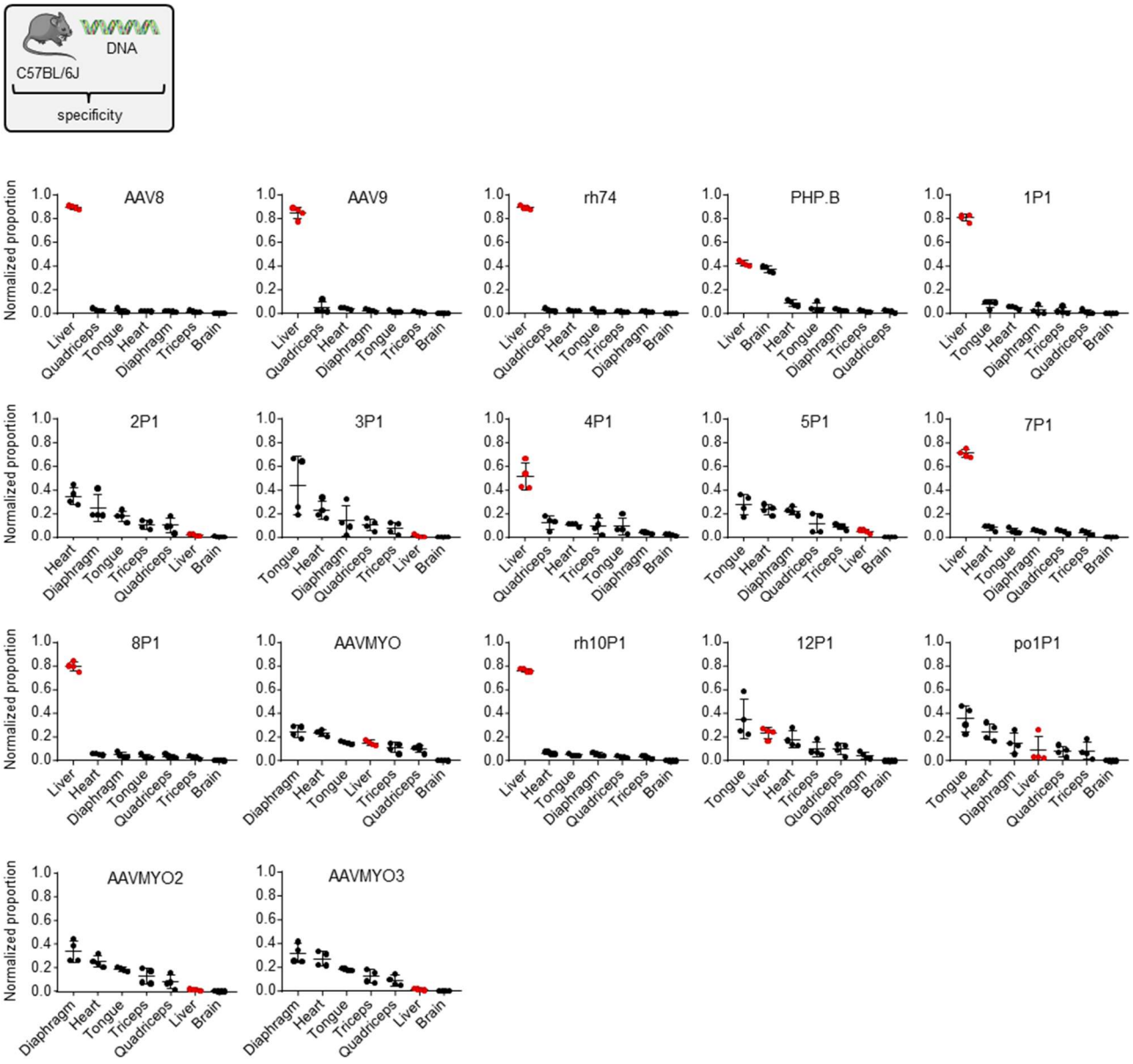

Fig. S9. Transduction specificity of P1-displaying AAVs in multiple tissues in C57BL/6J mice.

Depicted are normalized mean DNA values plus SD from four C57BL6/J mice. Liver samples are highlighted in red.

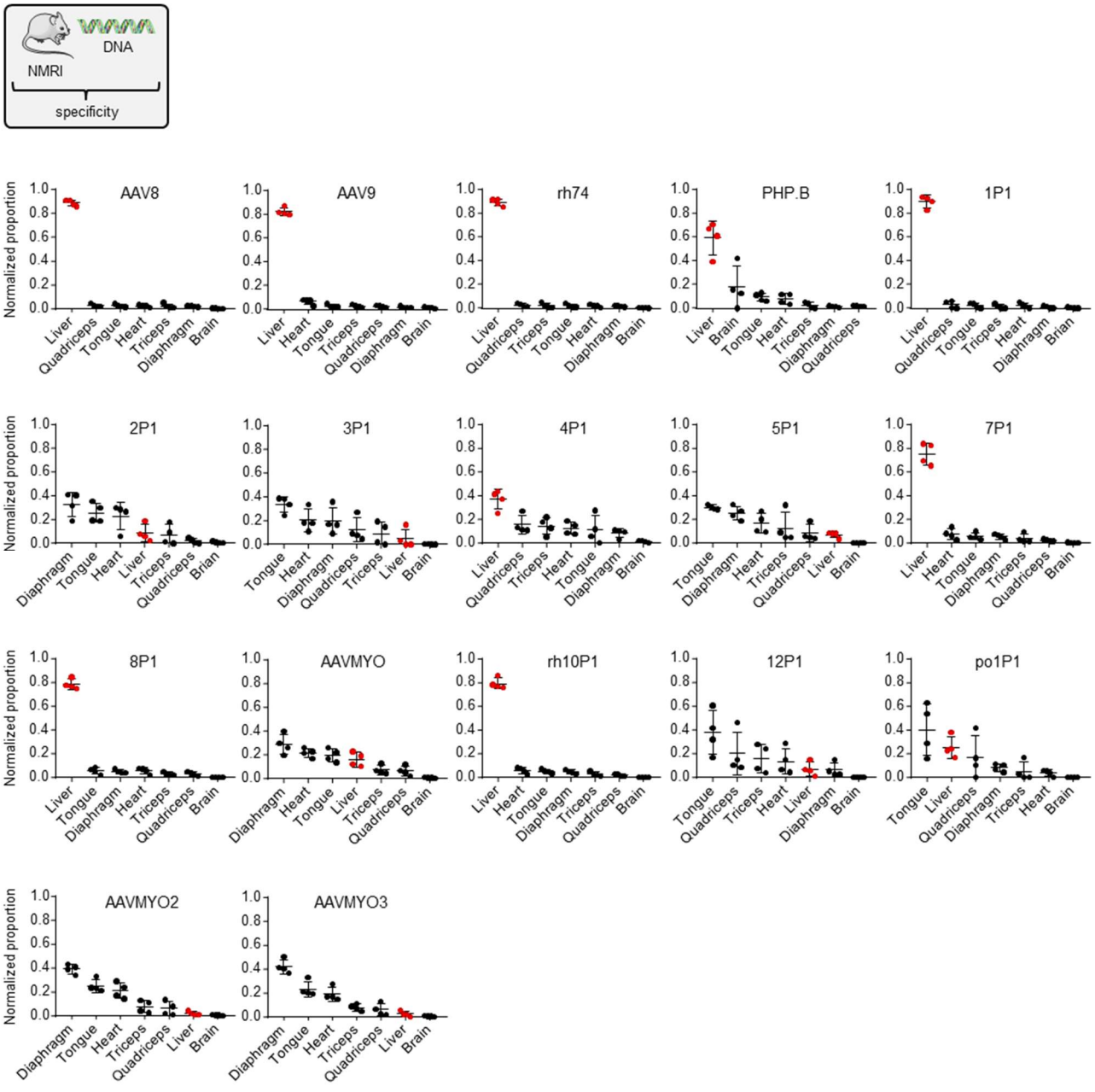

Fig. S10. Transduction specificity of P1-displaying AAVs in multiple tissues in NMRI mice. Depicted are normalized mean DNA values plus SD from four NMRI mice. Liver samples are highlighted in red.

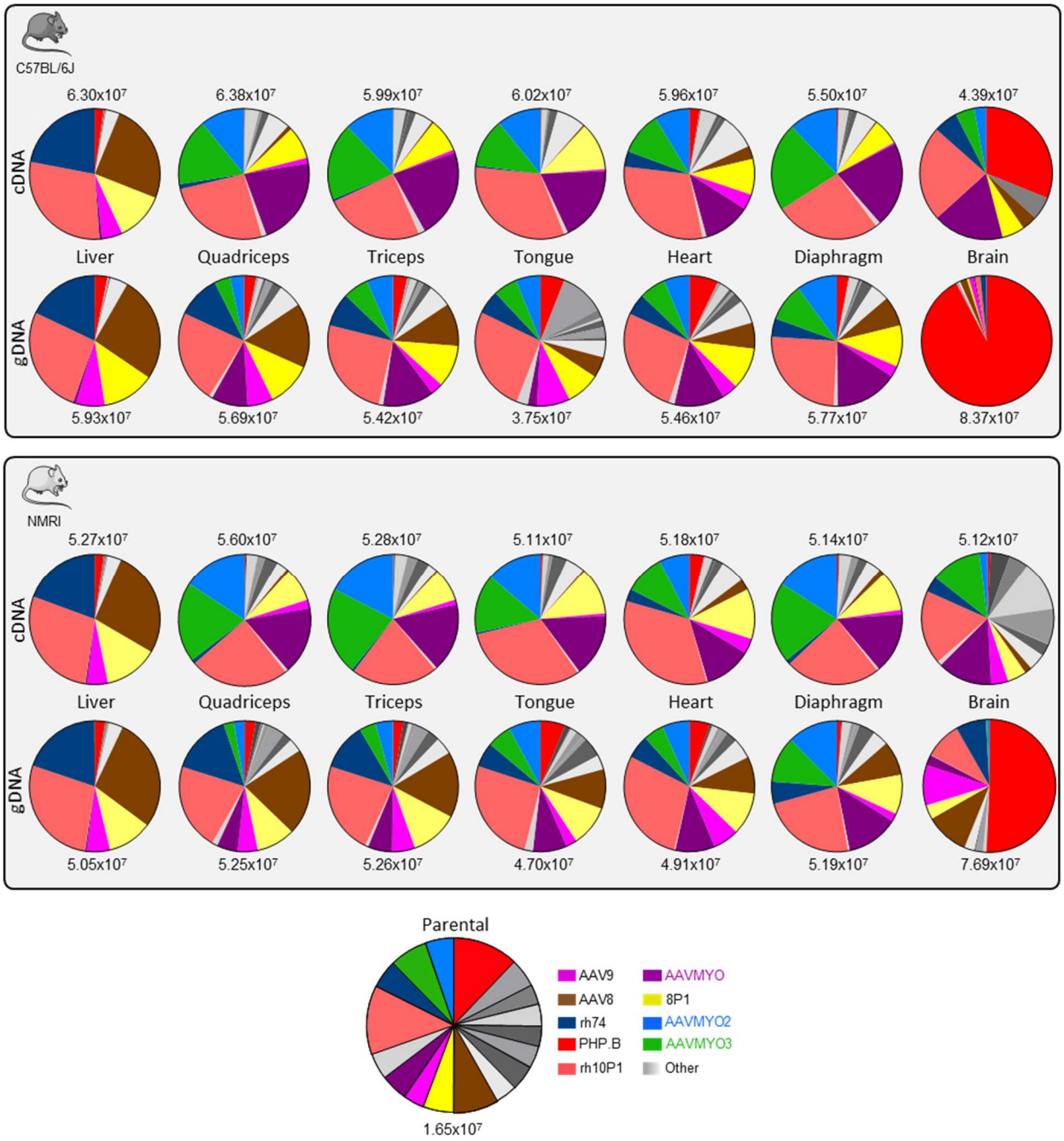

Fig. S11. Unique recovered reads in muscle tissues, liver and brain compared to the parental NGS library.

Pie charts depict the percentage of each capsid-specific barcode in a given tissue relative to the sum of all reads in this tissue. Total reads per tissue (numbers above or below the charts, respectively) was calculated as the sum of all reads in this tissue in all four C57BL/6J (top box) or NMRI (bottom box) mice, respectively. Total reads in the parental library is the sum of all recovered reads of the initial library that was injected into the mice. AAV variants of particular interest in this work are highlighted by colors.

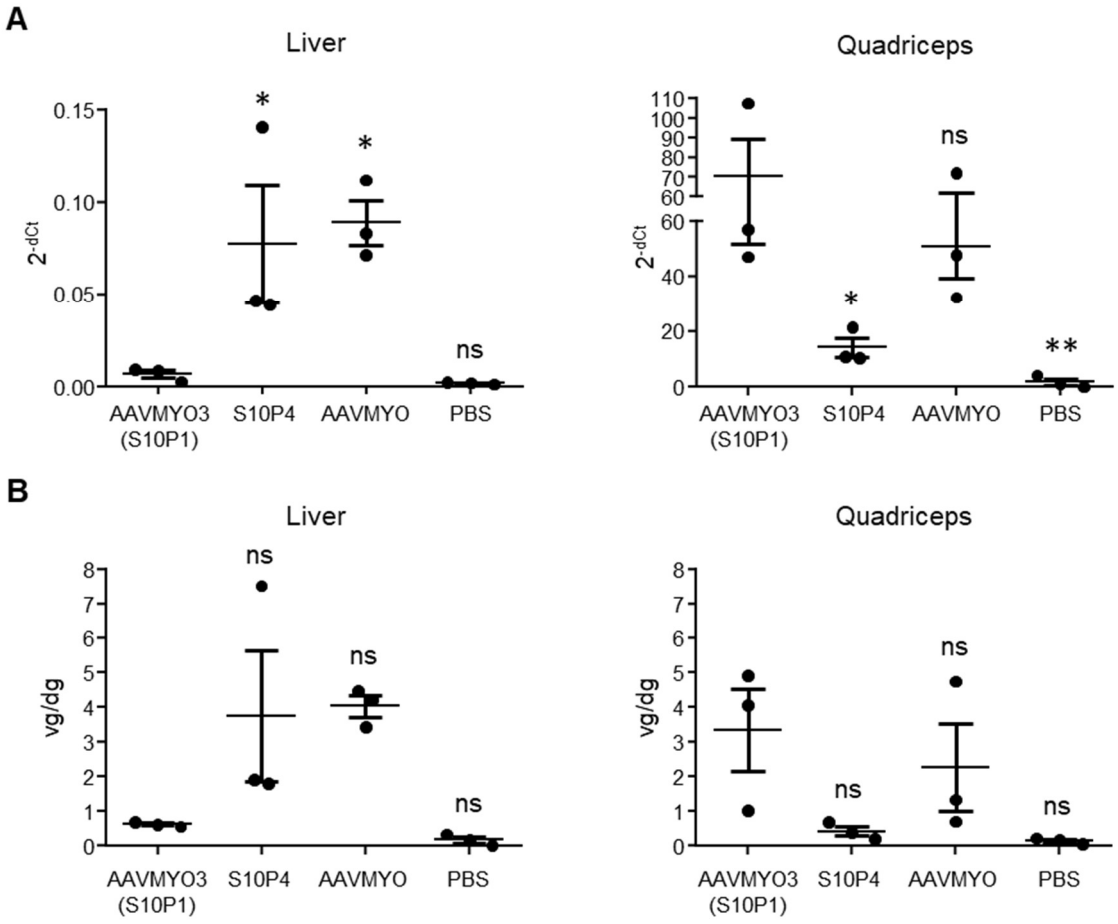

Fig. S12. Single validations of peptide-modified chimeras and benchmarks in liver and quadriceps femoris.

(**A**) Relative quantification (2^{-CT}) of cDNA values from eGFP and POLR2A of AAVMYO3 (AAVS10P1), AAVS10P4, AAV9, and AAVMYO which were individually injected at a dose of $3x10^{11}$ vg into the tail vein of three C57BL/6J mice. Incubation time was three weeks. (**B**) Vector genomes (vg) per diploid genome analyzed by ddPCR of eGFP and rpp30. Shown are means plus standard errors of the mean. Statistical analysis was performed using one-way Anova followed by Dunnet's multiple comparison post-test. All groups were compared against AAVMYO3. *p<0.05; **p<0.01. ns, not significant.

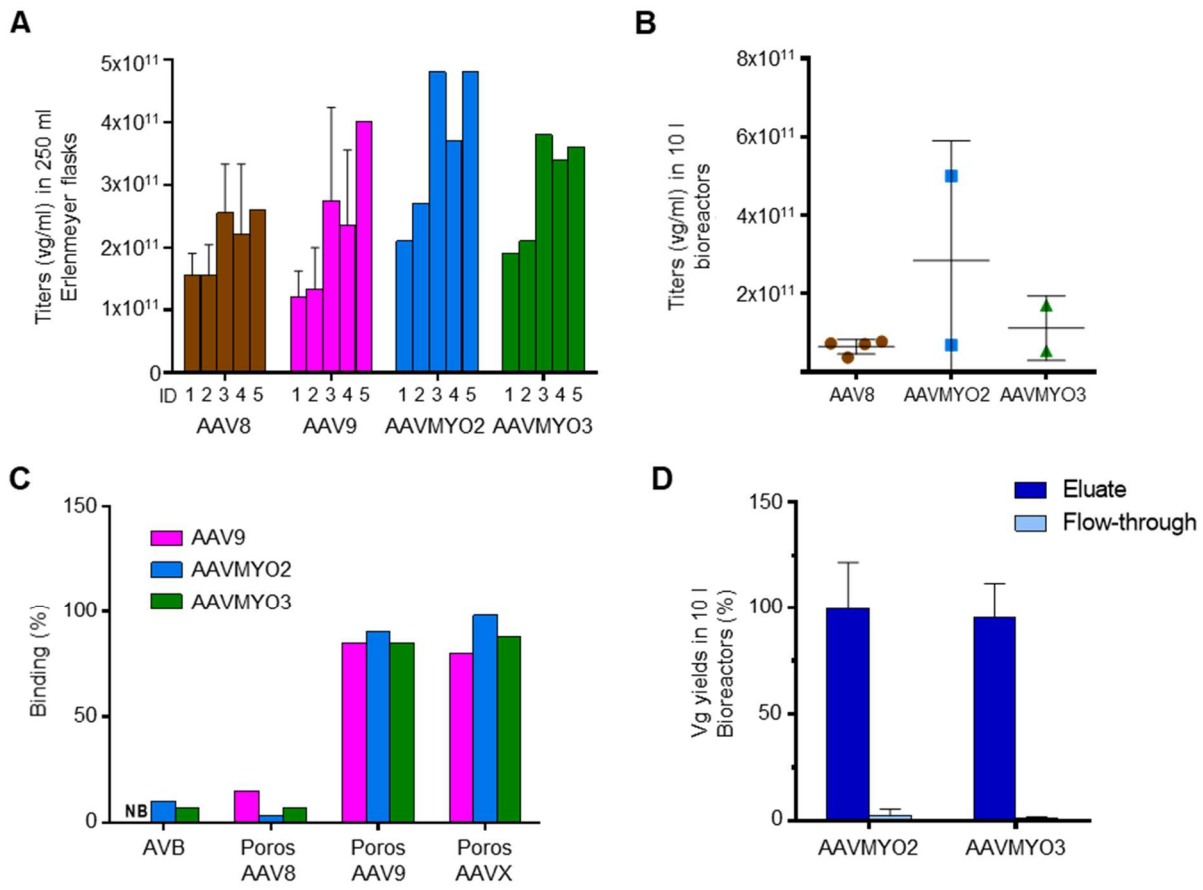

Fig. S13. Production and purification of AAVMYO2 and AAVMYO3.

(**A**) Results of packaging of five different AAV vector constructs (ID1 to ID5) into the shown four AAV capsid variants. Particles were harvested at 72 h post-transfection and quantified as vector genomes (vg) per ml by qPCR. n=1 or 2. (**B**) Results of vector production (n=2-4) in 10 l glass stirred tank reactors using the shown three AAV capsid variants. (**C**) Determination of the binding capability of the shown AAV capsid variants in a 96-well format to four different AAV purification resins (shown at the bottom). (**D**) Large-scale purification of AAVMYO2 and AAVMYO3 in a 10 l scale using the Poros AAVX resin.

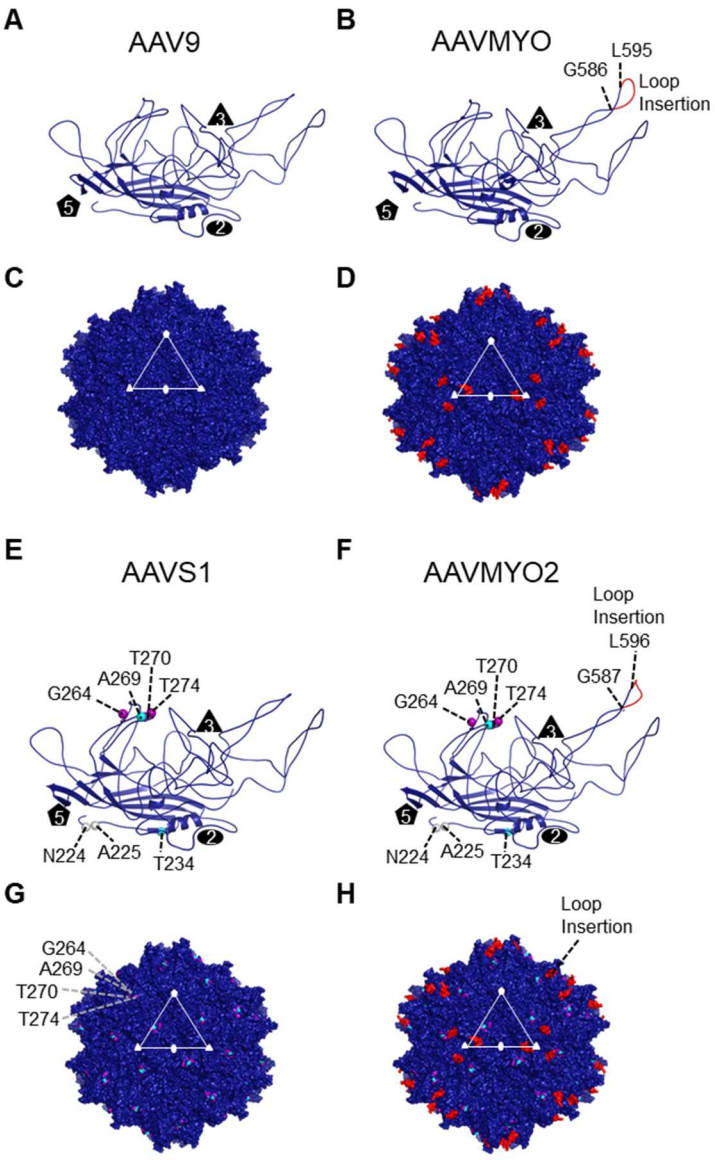

Fig. S14. AAV9, AAVMYO, AAVS1, and AAVMYO2 variant models.

Ribbon diagram of (**A**) AAV9, (**B**) AAVMYO, (**E**) AAVS1 or (**F**) AAVMYO2 VP3 monomer, along with surface representation of the (**C**) AAV9, (**D**) AAVMYO, (**G**) AAVS1 or (**H**) AAVMYO2 T=1 icosahedral capsids, using the same color scheme as in Figure 5. The position of the icosahedral 2-, 3- and 5-fold axes are shown as a black filled oval, triangle, and pentagon, respectively. Specific amino acids with the sequence and location equivalent to AAV9 are colored violet, and those similar to AAV1 and AAV6, and AAV8 are colored as gray, teal and purple spheres, respectively. In addition, the peptide insertion P1 at VR VIII from G585-L594 is colored red in (**B**, **D**, **F**, **H**). The surface features show the characteristic 2-fold depression at the 2-fold axes, 3-fold protrusions surrounding the 3-fold axes, the 2/5-fold wall and the 5-fold pore forming the 5-fold axes. The 2-fold, 3-fold and 5-fold axes are labeled as white filled oval, triangle and pentagon, respectively. The figures were generated using the program Pymol.

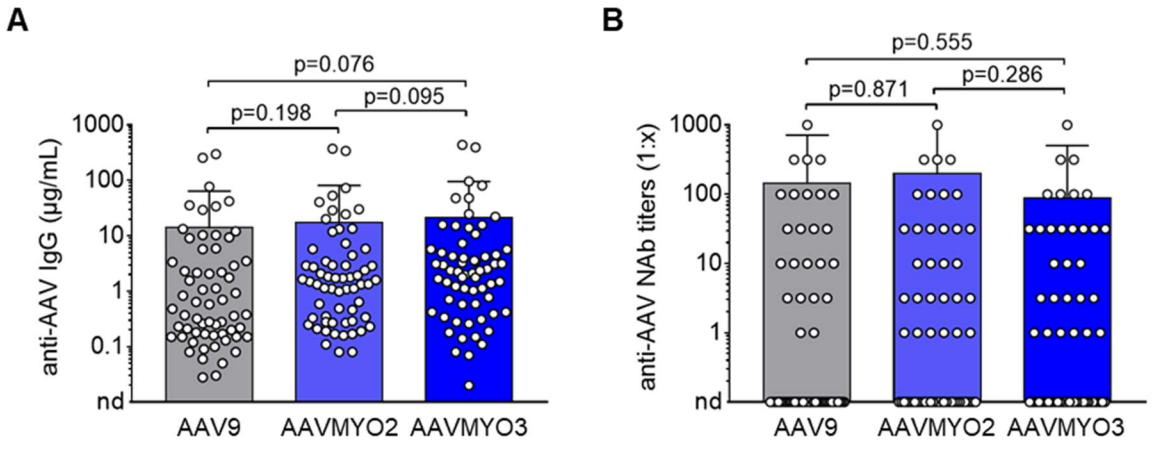

Fig. S15. Immunoreactivity of AAVMYO2 and AAVMYO3.

Prevalence of anti-AAV9, anti-AAVMYO2 and anti-AAVMYO3 antibodies in a cohort of 63 human serum samples. (**A**) Binding antibodies measured by ELISA. (**B**) Neutralizing antibody titers measured by in vitro neutralization test. Data are mean ± SD. Statistical analyses were performed by one-way ANOVA with Tukey's multiple comparisons test (n=63).

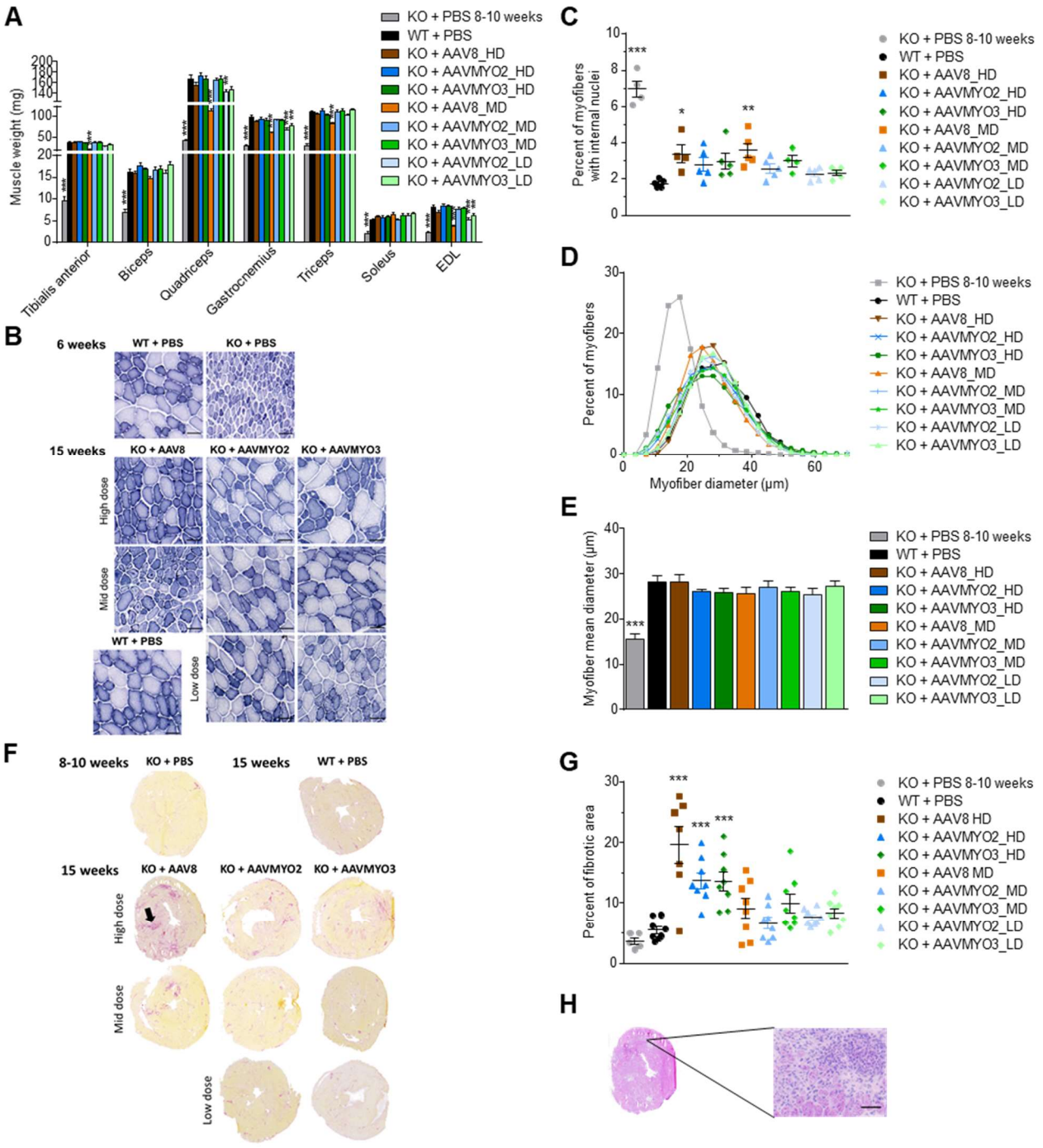

Fig. S16. Muscle weight and histological findings in Mtm1-KO mice three months after AAV8, AAVMYO2 and AAVMYO3 delivery at various doses.

(**A**) Weight of several muscles untreated KO mice at 8 to 10 weeks of age (n=10) or WT and treated KO mice at 15 weeks of age (n=8, except for KO + AAV8_HD n=7). EDL: Extensor Digitorum Anterior Longus. (**B**) Cross-sections from tibialis anterior (TA) stained with NADH-

TR from wild-type (WT, at 6 and 15 weeks) and KO mice injected with PBS (at 6 weeks) or AAV8, AAVMYO2 or AAVMYO3 at $1.0x10^{14}$ vg/kg (HD), $2.0x10^{13}$ vg/kg (MD) or $4.0x10^{12}$ vg/kg (LD) at 15 weeks of age. Scale bars = 50 µm. (**C**) Percentage of centronucleated fibers in biceps. (**D**) Biceps myofiber diameter frequency distribution. (**E**) Biceps myofiber mean diameter. n=5 per group at 15 weeks (except for KO + AAV8_HD n=4, and KO + PBS at 8 to 10 weeks n=4). (**F**) Cross-sections from heart stained with Sirius red. The black arrow indicates a fibrotic area. (**G**) Quantification of collagen deposition (fibrotic area/total section area). n=5 for KO + PBS at 8 to 10 weeks and n=8 for WT and treated KO mice at 15 weeks (except for KO + AAV8_HD n=7). (**H**) Representative cross-section of heart stained with hematoxylin-eosin (HE) from an AAV8_HD KO mouse at 15 weeks of age, with higher magnification of a region containing cellular infiltrates (scale bar 50 µm). Mean is represented ± standard error of the mean. Statistical analyses were performed by using one-way ANOVA followed by Dunnet's multiple comparison post-test: * $p<0.05$; ** $p<0.01$; *** $p<0.001$ versus WT + PBS.

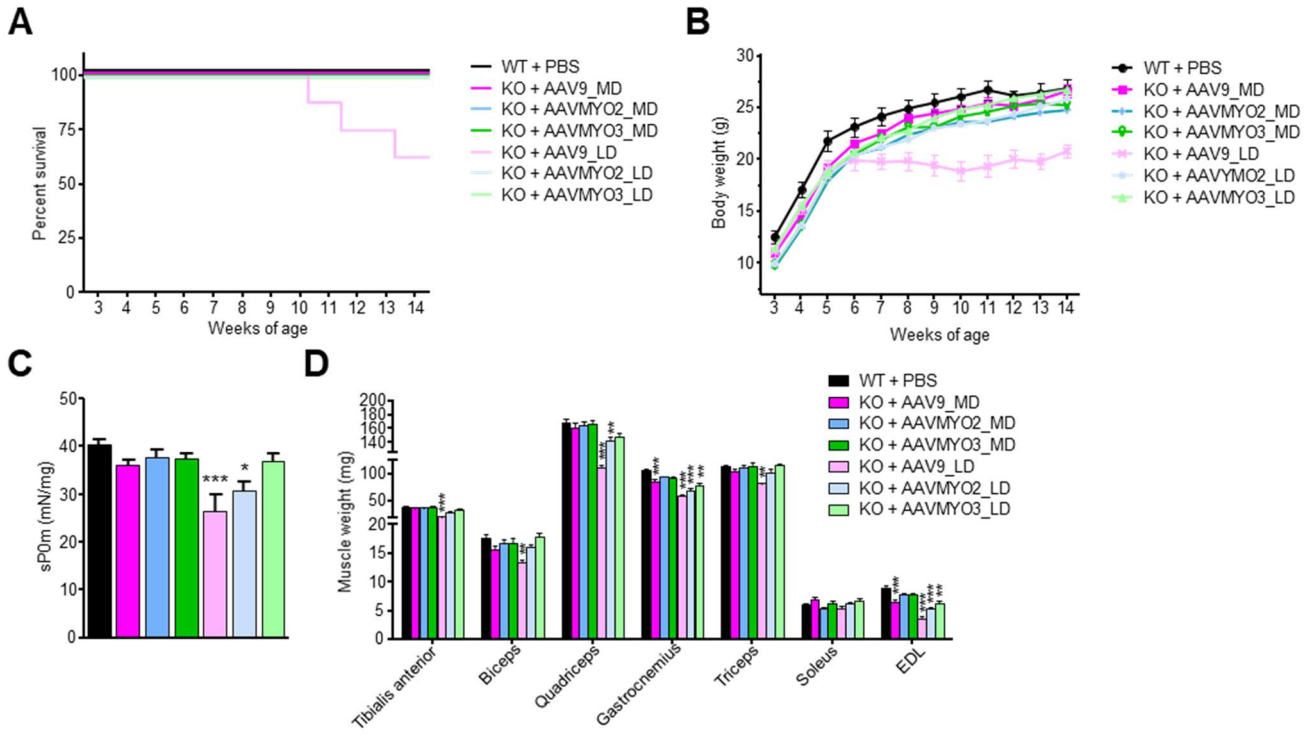

Fig. S17. Lifespan, body growth, strength and muscle weight in Mtm1-KO mice after AAV9-MTM1 delivery.

(**A**) Survival rate and (**B**) body weight of wild-type (WT, n=6) and KO mice injected with either PBS or AAV9-MTM1 at $2.0x10^{13}$ vg/kg (MD, n=8) and $4.0x10^{12}$ vg/kg (LD, n=8) over a 3-month study period. (**C**) Specific tetanic force of tibialis anterior muscles from WT or treated KO mice at 15 weeks of age (WT n=6, AAV9_MD n=8, AAV9_LD n=4). (**D**) Weight of several muscles from WT and treated KO mice at 3 months after injection (WT n=6, AAV9_MD n=8, AAV9_LD n=5). EDL: extensor digitorum longus. Mean is represented ± standard error of the mean. Statistical analyses were performed by using one-way ANOVA followed by Dunnet's multiple comparison post-test, at 15 weeks: ** $p<0.01$; *** $p<0.001$ versus WT + PBS. The data of KO mice treated with AAVMYO2- and AAVMYO3-MTM1 vectors at MD and LD are the same than in Figure S16, and are included in this figure to facilitate the comparison with AAV9-MTM1 vector administration.

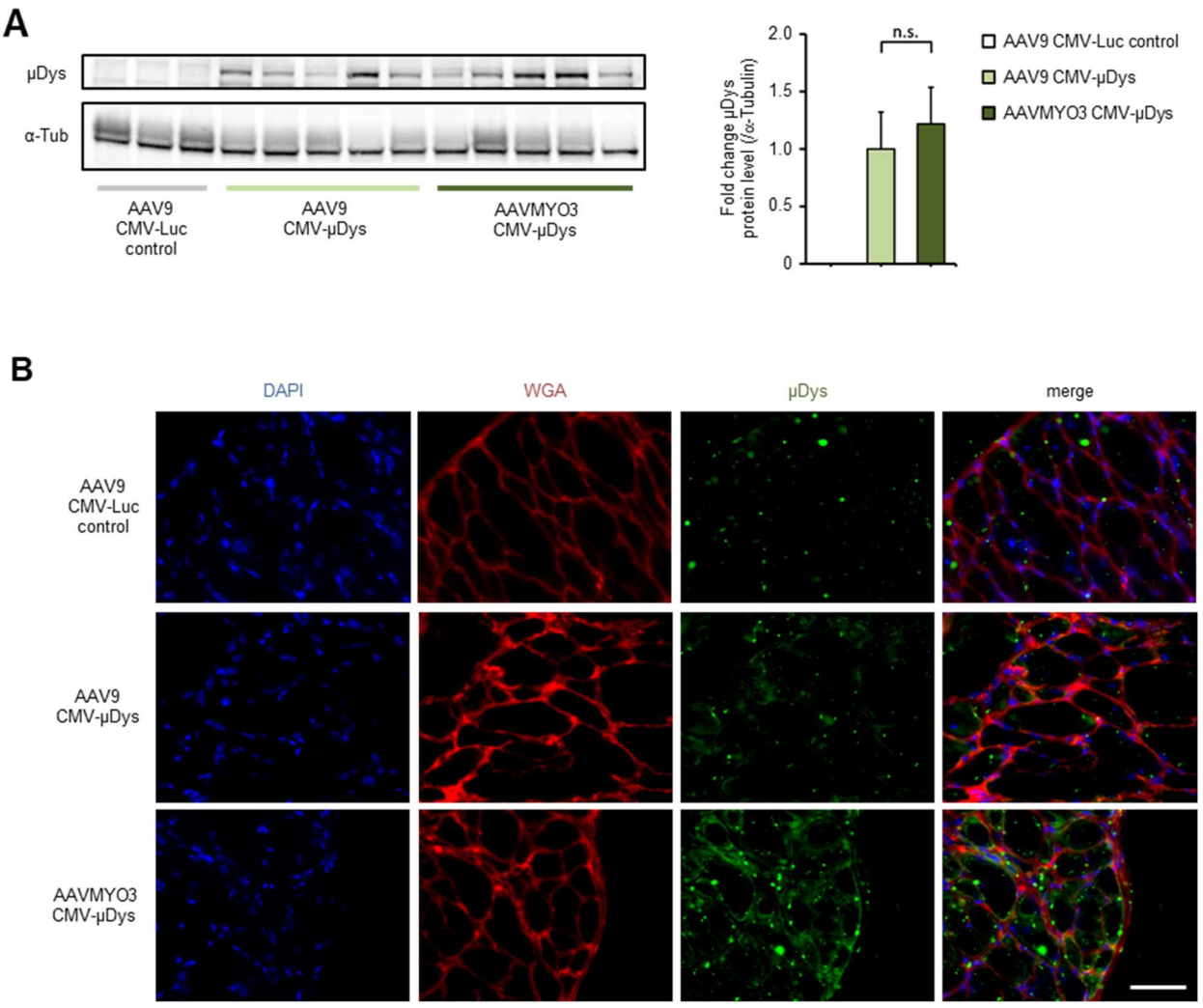

Fig. S18. Additional validation of micro-Dystrophin (μDys) expression from AAVMYO3 in *mdx* mice.

(**A**) Immunoblot with densitometry analysis showing μDys expression in cardiac tissue of *mdx* mice 23 weeks after i.v. injection of $2x10^{12}$ vg of control vector (AAV9 Luc expressing luciferase, n=3), or of AAV9 or AAVMYO3 encoding μDys under the control of the CMV promoter (n=5 per group; loading control α-Tubulin). Mean is represented + standard error of the mean. (**B**) Comparison of AAV-mediated μDys expression in diaphragm sections of the same *mdx* mice as in panel A. Scale bar 50 μm.